Metallurgical and Materials Engineering *Research paper*
Association of Metallurgical Engineers of Serbia AMES *https://doi.org/10.30544/824*

DRY SLIDING WEAR BEHAVIOR AND ITS RELATION TO MICROSTRUCTURE OF ARTIFICIALLY AGED Al-Si-Mg/TiB_2 IN SITU COMPOSITES

Nishith Rathod[1], Jyoti Menghani[2]*

[1] Department of Mechanical Engineering, C K Pithawala College of Engineering and Tech., Surat, India.
[2] Department of Mechanical Engineering, Sardar Vallabhbhai National Institute of Technology, Surat, India.

Received 10.11.2021

Accepted 17.06.2022

Abstract

Mechanical stir casting is utilized to produce an artificially aged Al-Si-Mg alloy, whereas halide slat (K_2TiF_6 and KBF_4) synthesis is utilized to produce Al-Si-Mg/TiB_2 aluminum matrix composites. The dry sliding pin on disc wear test was conducted using a DUCOM/TR-20LE-PHM-200 machine to simulate an automobile application (Piston-Ring assembly). Where pistons are made of aluminum alloy (for the Pin) and rings are made of grey cast iron (for the disc material). At room temperature, a wear test was conducted by altering the ageing time (3, 6, 9, 12), sliding speed (2, 2.5 m/s), and applied load (14.71, 19.62, 24.52 N) with the disc speed (500 rpm) held constant (10 min). The results indicate that the aluminum matrix composite (AMC) wear rate is reduced by 37 percent at higher sliding speeds (2.5 m/s) and by 4 percent at lower sliding speeds (2.0 m/s) compared to the base alloy. Field emission scanning electron microscope-energy dispersive spectroscopy (FESEM-EDS) and X-ray photoelectron spectroscopy (XPS) analysis revealed that the formation of the mechanically mixed layer (MML) or oxidative layers on the worn surfaces reduces the wear rate under conditions of longer ageing time, higher sliding speed, and lower applied load. The research demonstrates that composite wear is a function of sliding velocity, aging period, and applied force. As sliding speed rose from 2 m/s to 2.5 m/s, the wear rate of composites dropped reasonably, yet composites are softer than basic alloys. It is conceivable due to the presence of a considerable amount of MML and the formation of oxidative layers between pins and their equivalents.

Keywords: TiB_2; artificially aged; dry sliding wear; mild wear; MML.

[*] Corresponding Author: Nishith Rathod, *nishtih11679@gmail.com*

1. Introduction

The huge growth in demand for fuel-efficient and lightweight materials in the automotive and aviation industries has led to a surge in the development and design of new, custom-made materials. Due to their remarkable corrosion resistance, high ductility, high strength-to-weight ratio, and low cost, Al-Si-Mg master alloys are one of the most widely used alloys in the vehicle industry. These materials, however, have poor tribological properties [1]. Therefore, alloy modification and improved mechanical and tribological responses are required, which will eventually lead to the development of aluminum metal matrix composites (AMC). Metal matrix composites (MMC) exhibit exceptional rigidity, abrasion resistance, and strength enhancement. Aluminum metal matrix composites have numerous applications in the engineering, marine, automotive, and aerospace sectors. Oxides [2], borides [3], nitrides [4], and carbides [3] are the most frequently used reinforcements for application-specific MMC.

In-situ or ex-situ particle reinforcement could significantly improve the tribological properties of the Al-Si system [5]. Conventional composite fabrication is accomplished by reinforcing hard particles in pure metals and/or metal alloys, termed ex-situ MMCs. SiC, TiC, TiB_2, ZrB_2, B4C, and Al_2O_3 are some of the most prevalent reinforcing elements that, in addition to enhancing wear resistance and mechanical properties, also serve as heterogeneous nucleation sites, resulting in grain refinement. These reinforcing particles are lightweight and possess high hardness and melting points. They function as dispersion strengthening agents, impede dislocation motion, and increase the strength of AMC. These AMCs are ideal for aircraft and automotive components such as pistons, gears, cylinder liners, clutches, and engine block housing [6]. TiB_2 is one of the most widely used reinforcements due to its exceptional mechanical and physical properties, including its exceptional hardness, high melting point, high elastic modulus, and exceptional wear resistance. TiB_2 particles added to an Al matrix reportedly stimulate heterogeneous nucleation of α-Al and have a favorable crystallographic orientation relationship that results in high coherency and low solid particle interfacial energy [7]. An approach was to develop reinforcement particulates via chemical reaction within a liquid or solid at a higher temperature, known as the salt synthesis route (in situ route). The in situ route has significant advantages against the ex-situ route like outstanding bonding strength, clean matrix-reinforcement interface, thermodynamically stable and fine grain structure, good wettability, and minimum processing cost. A significant parameter that influences the properties of AMC is the chemical reaction between the reactants of the solution and the holding time of response. TiB_2, TiC, and Al_2O_3 are the most common reinforcements fabricated by the salt synthesis route because they are not reacting with the matrix [8].

The researchers devoted a substantial amount of effort to the Al-Si-Mg system strengthened with SiC particles [5]. However, few studies on wear of AMCs reinforced via salt synthesis route (in-situ route) with TiB_2 particles have been published [2, 3]. *Rathod N. R.*, & *Menghani J.* (2019) and *P. Samal et al.* (2020) advocated the advantageous effect of in-situ TiB_2 particles [2, 3]. In addition, no aluminum-based intermetallics or reaction products are formed near the interface of the matrix and reinforcement [9, 10]. Moreover, Al/TiB_2 AMCs prepared by the salt synthesis route have recently been cited with improved mechanical and tribological properties [11].

Precipitation hardening is an additional technique for fortifying Al-Si-Mg alloy. In recent years, researchers have devoted a substantial amount of time and energy to

studying the effects of precipitation hardening on aluminum-based systems. The precipitation-hardening process is attained by heating a supersaturated solid solution at elevated temperature followed by quenching in different media and natural ageing processes (ageing occurs at room temperature) or artificial ageing process (ageing takes place at high temperature). The solution heat treatment followed by aging is crucial for increasing the mechanical properties and durability of metallic components [12]. The precipitation sequence in the Al-Mg-Si system is represented as follows;

Clusters of Si atoms → GP-I zones (primary monoclinic) → GP-II- zones (β")
(needle shape) → β' (hexagonal) → β' (Mg_2Si)

First, the decomposition of the system starts and passes through different unstable phases (called GP zones), and in the last stage, the system ultimately losses coherency, and the equilibrium β (Mg_2Si) phase is formed [13]. The storage time (aging time), temperature, and alloy composition are crucial factors that influence the performance of aged aluminium-based systems [14]. The peak aged AMC demonstrates the greatest resistance to wear under both over-aged and under-aged conditions [15].

The wear behavior of AMC is determined by the type and size of reinforcements, the microstructure of the system, and the wear governing parameters. This study examines the wear of four types of samples: (a) base alloy (Al-Si-Mg system), (b) artificially aged Al-Si-Mg system, (c) Al-Si-Mg/TiB_2 in situ composites fabricated by salt synthesis route, and (d) artificially aged Al-Si-Mg/TiB_2 in situ composites fabricated by salt synthesis route. Two steps of artificial ageing treatment; (a.) Solutionizing treatment (b.) Artificially ageing (varying times 3, 6, 9, 12 hours) incorporates the test samples. ASTM - G99 standard is used to perform the pin on disc wear test to record dry sliding wear responses. The wear test used different sliding speeds (2, 2.5 m/s) and normal applied load (14.71, 19.62, 24.52 N). To incorporate wear response and hardness of both categorical samples (base alloy and composites) BHN hardness test is performed as per ASTM E10-14 standards. The microstructure and surface morphology of worn surfaces incorporate by X-ray diffraction (XRD), Field emission scanning electron microscope-energy dispersive spectroscopy (FESEM-EDS) and X-ray photoelectron spectroscopy (XPS) analysis.

2. Materials and methods

2.1 Processing of in situ composites

The commercial Al-7Si-0.3Mg master alloy was heated up to 850 ºC, and two halide salts (KBF_4 and K_2TiF_6) were added to the molten Al-7Si-0.3Mg system in the atomic ratio of Ti:2B by the mechanical stirring method. A ceramic stirrer stirs the melt. The exothermic reaction between the two halide salts and the molten Al-7Si-0.3Mg system resulted in situ TiB_2 particles in the Al-7Si-0.3Mg system. The reaction holding time and the exothermic reaction temperature are 45 minutes and 850 ºC, respectively. Fig. 1, flow process chart represents fabrication of in situ composites via salt synthesis route [16].

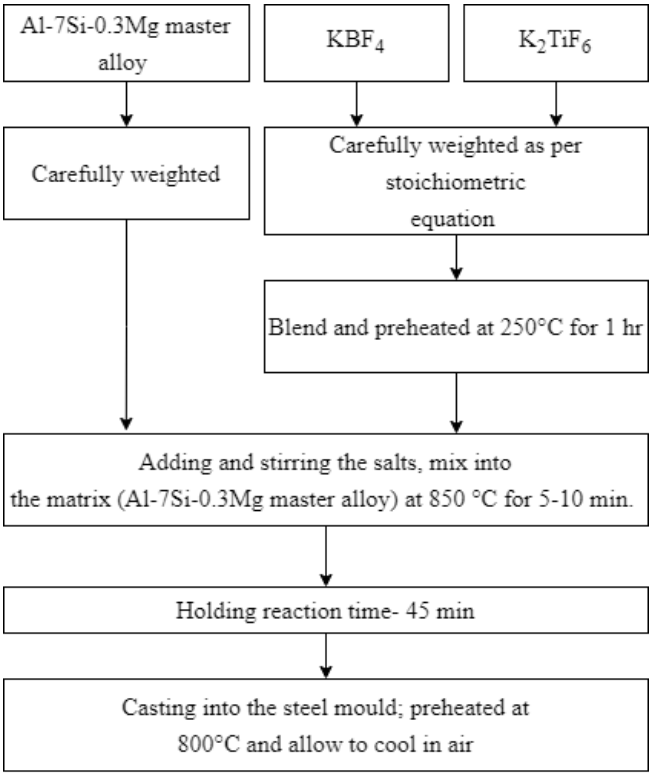

Fig. 1. Flow process chart of the in situ process used for synthesizing Al-7Si-0.3Mg/TiB_2 composite.

2.2 Heat treatments

The Al-Si-Mg system with and without TiB_2 was artificially aged. Solutionizing heat treatment was attempted at 501 ºC for 1 h [17], followed by water quenching and single-stage artificial ageing at 175 °C for different ageing times (3, 6, 9, 12 h).

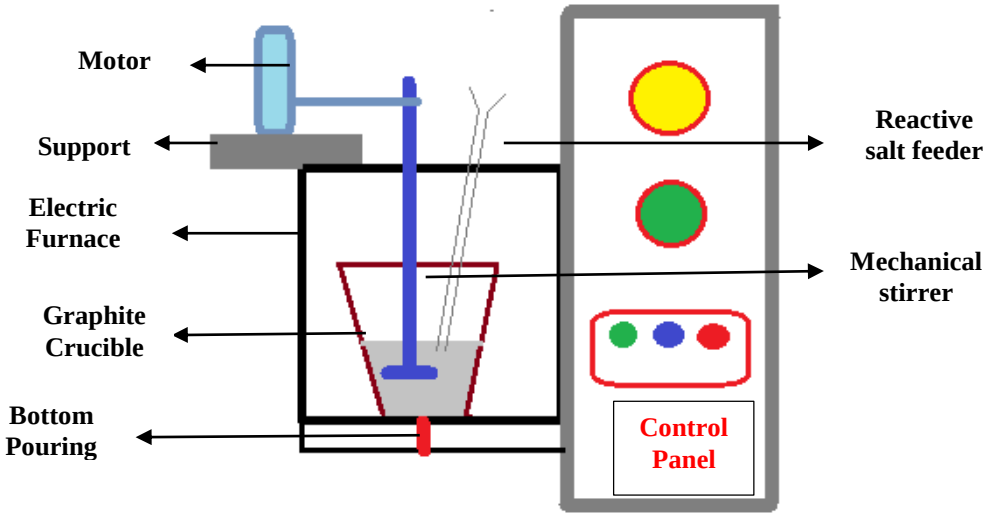

Fig. 2. Schematic diagram of bottom pouring mechanical stir casting furnace.

2.3 Pin on disc wear test

DUCOM/TR-20LE-PHM-200 machine incorporate to perform the dry sliding pin on disc wear test. The fabrication of test sample is as per ASTM - G99, cylindrical pin (30 mm height and 10 mm diameter) of the Al-Si-Mg system (with and without ageing treatment and with and without TiB_2). This paper aims to replicate the piston ring assembly application, where the fabrication process of a commercial piston from the Al-Si-Mg system and its AMC (Al-Si-Mg/TiB_2) and the disc from grey cast iron. In context, an artificially aged Al-Si-Mg master alloy and AMC (Al-Si-Mg/TiB_2) are used to fabricate cylindrical pin and grey cast iron (Brinell HB 224) is used to manufacture the counterpart (the disc). Pin on disc wear test is carried out at different sliding speeds (2, 2.5 m/s) and normal applied load (14.71, 19.62, 24.52 N). The counterpart (disc) rotation speed and time, 500 rpm and 10 minutes, remain constant for all samples. In the absence of lubrication conditions, an ambient environment is used for all wear tests. FESEM-EDS and XPS studies of the Al-Si-Mg system and Al-Si-Mg/TiB_2 AMCs carried out for worn samples. Weight loss assessment technique used for calculating the amount of wear rate for given samples.

$$\text{Wear rate, } (mm^3/m) = \text{Volume loss/ sliding distance} \quad (1)$$

$$\text{Volume loss, } (mm^3) = \text{Mass loss/ density} \quad (2)$$

Where density in g/cm^3.

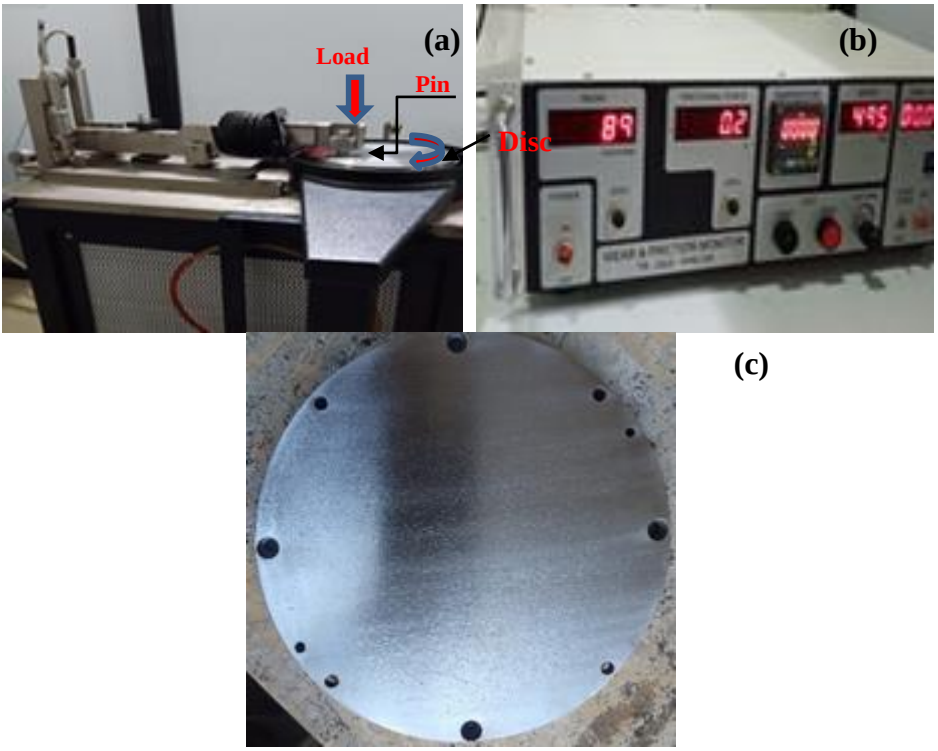

Fig. 3. (a) Pin on Disc apparatus, (b) Data acquisition system and (c) Disc (made of gray cast-iron).

Result and discussion

3.1 Formation and examination of TiB_2 in situ composites

The following chemical reaction represents the formation of TiB_2 particles through in situ route.

$$K_2TiF_6\,(1) + KBF_4\,(1) + Al\,(1) \longrightarrow TiB_2\ (\text{in alloy}) + KFAlF_3\,(1) + KF\,(1) + AlF_3\,(1) \quad 3$$

To confirm the presence of TiB_2, a Panalytical Xpert X-ray diffraction machine was used to conduct an XRD test. Fig. 4 depicts the XRD (X-ray diffraction) analysis plot. Along with Al and Si, the corresponding peaks of TiB_2, AlB_2, and Al_3Ti are also reported. At high temperatures (850 °C), both halide salts (KBF_4 and K_2TiF_6) decompose, and the decomposed elements K and F form slag on the surface of the aluminum melt. Given a molten state, the ternary system Al-Ti-B is theorized to exist. The research revealed that the formation of TiB_2 occurs at 1023 K (750 °C). However, as the reaction temperature rises, the Gibbs' free energy of TiB_2 rises and the system's TiB_2 formation rate increases.

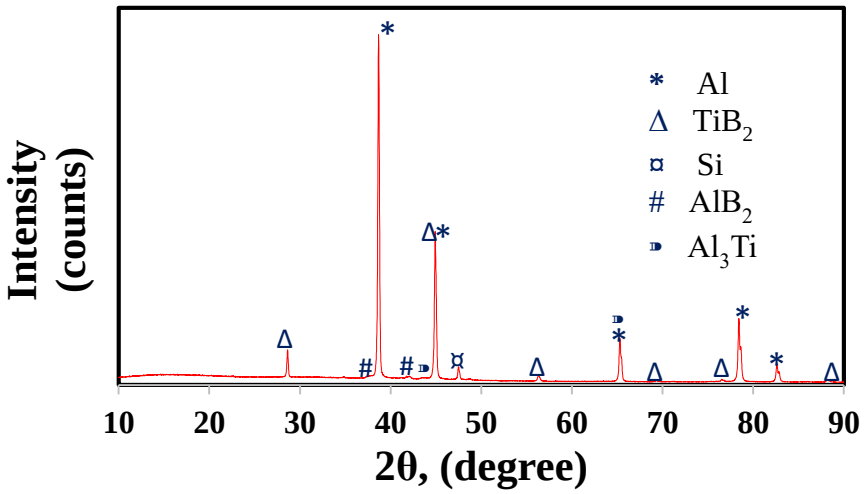

Fig. 4. XRD plot of Al-Si-Mg/TiB_2 in situ composites fabricated by salt synthesis route.

Theoretically, as the reaction temperature rises, the decrease in Gibbs free energy of Al_3Ti decreases, indicating that Al_3Ti is unstable [18]. Consequently, TiB_2 increased, Al_3Ti decreased, and more Ti was converted to the TiB_2 phase [19].

Figure 5 illustrates the FESEM-EDS image and its mapping of composite (Al-Si-Mg/TiB_2) in order to comprehend and validate XRD peaks. In Fig. 4, the intensity of the AlB_2 and Al_3Ti peaks is weak. At some point, the Al_3Ti peak overlaps the Al peak. FESEM-EDS mapping verifies whether or not secondary phases AlB_2 and Al_3Ti formed during the salt reaction. Nonetheless, this observation does not indicate any secondary phase. This analysis makes it simple to exclude elements of the secondary phase and their detrimental effect on the material to exempt the secondary phase elements and its detrimental effect on the material.

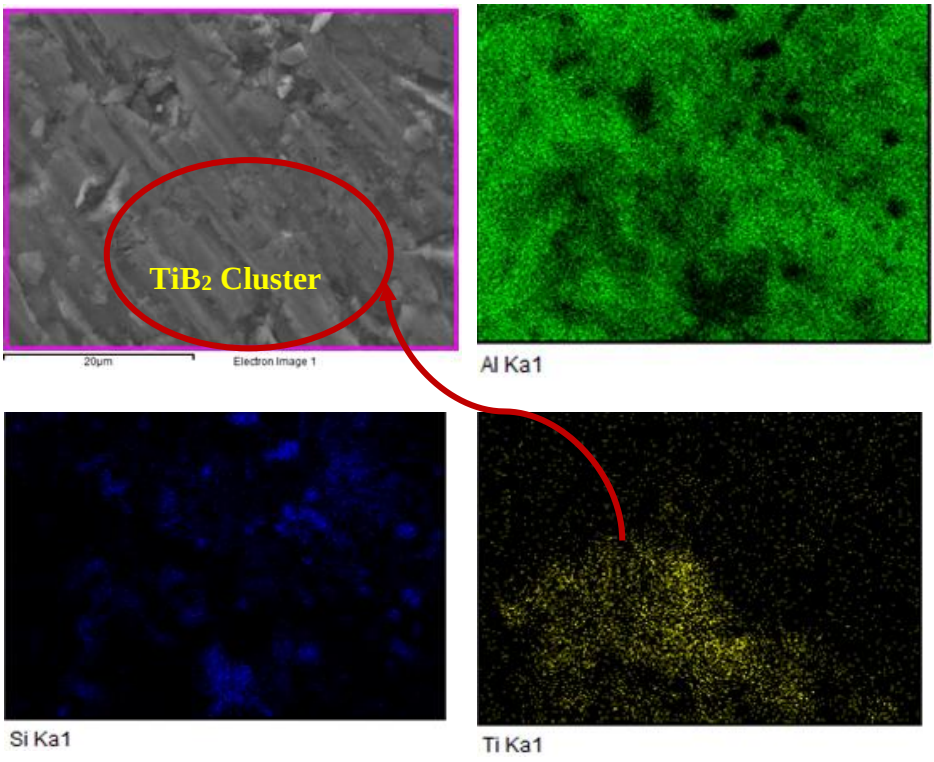

Fig. 5. FESEM-EDS image and its mapping of composites (Al-Si-Mg/TiB_2).

3.2 Quantification of BHN (hardness)

The ASTM E10-14 standard is utilized for the BHN hardness test. It measures the average value of five indentation centers to surface under a 500kgf load with a 10 mm indenter.

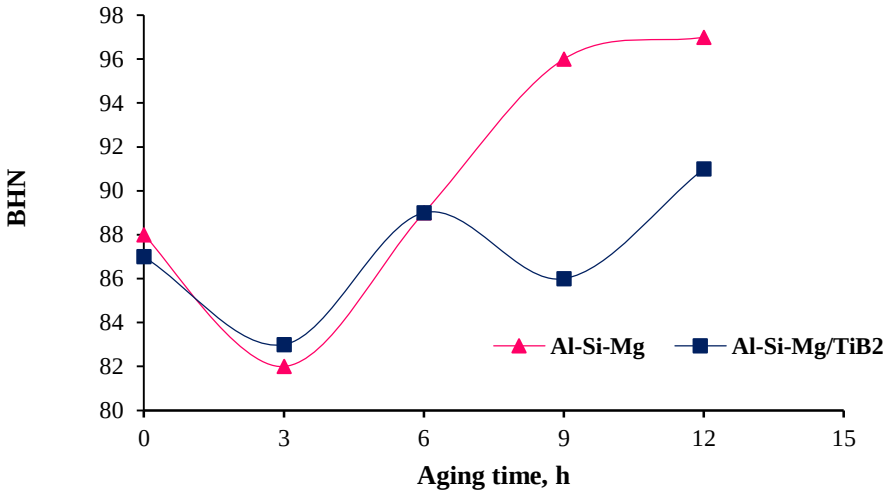

Fig. 6. Effect of aging time on BHN, base alloy (Al-Si-Mg) and Composite (Al-Si-Mg/TiB_2).

The BHN test revealed that the composites and base alloys have identical hardness under non-aging conditions. However, as ageing time increases, composites become softer than base alloy in the same condition up to 9 h ageing time, but thereafter, grain refinement during 12 h ageing improves hardness. The particle size of TiB_2 is crucial to the hardness of composites. According to reports, the grain growth of TiB_2 particles is affected by reaction holding time. Up to 30 minutes of reaction holding time reveals the optimal particle size of TiB_2 via the salt synthesis route. However, grain size increased as reaction holding time increased beyond 40 minutes [3]. However, after 40 minutes, the brittle secondary element Al_3Ti is completely dissolved and converted into TiB_2 particles (In this study, the reaction holding time is 45 minutes).

3.3 Quantification of wear rate of base alloy and composites

3.3.1 Effect of sliding speed, aging time and normal applied load on wear behaviour

The wear rate of base alloy (Al-Si-Mg - A1) and AMC (Al-Si-Mg/TiB_2 -A2) as a function of ageing time (3, 6, 9, 12 h) for sliding speed and normal applied load is illustrated in Figure 7. This study examined sliding speeds of 2, 2.5 m/s and normal applied loads of 14,71, 19,62, and 24,52 N. As shown in Fig. 7 (a), (b), and (c), as sliding speed increased from 2 to 2.5 m/s, wear rate decreased at 14.71 N and 24.52 N normal load as ageing time increased. With the exception of 19.62 N, the wear rate at 2 m/s sliding speed is less than 2.5 m/s. Al-Si-Mg/TiB_2 AMC, on the other hand, exhibits a steady decrease in wear as ageing time increases for normal loads of 14.72 N and 19.62 N (Fig. 7(d) and (e)). There is an initial decrease followed by an increase in wear for 24.52 N. At longer ages, the rate of deterioration is observed to decrease steadily in all

instances. The sliding speed increased to 2.5 m/s and the amount of wear decreased compared to 2 m/s for all loading conditions as a result of aging. According to the discussion, it is evident that as ageing time increases, the achieved wear rate decreases at higher sliding speeds.

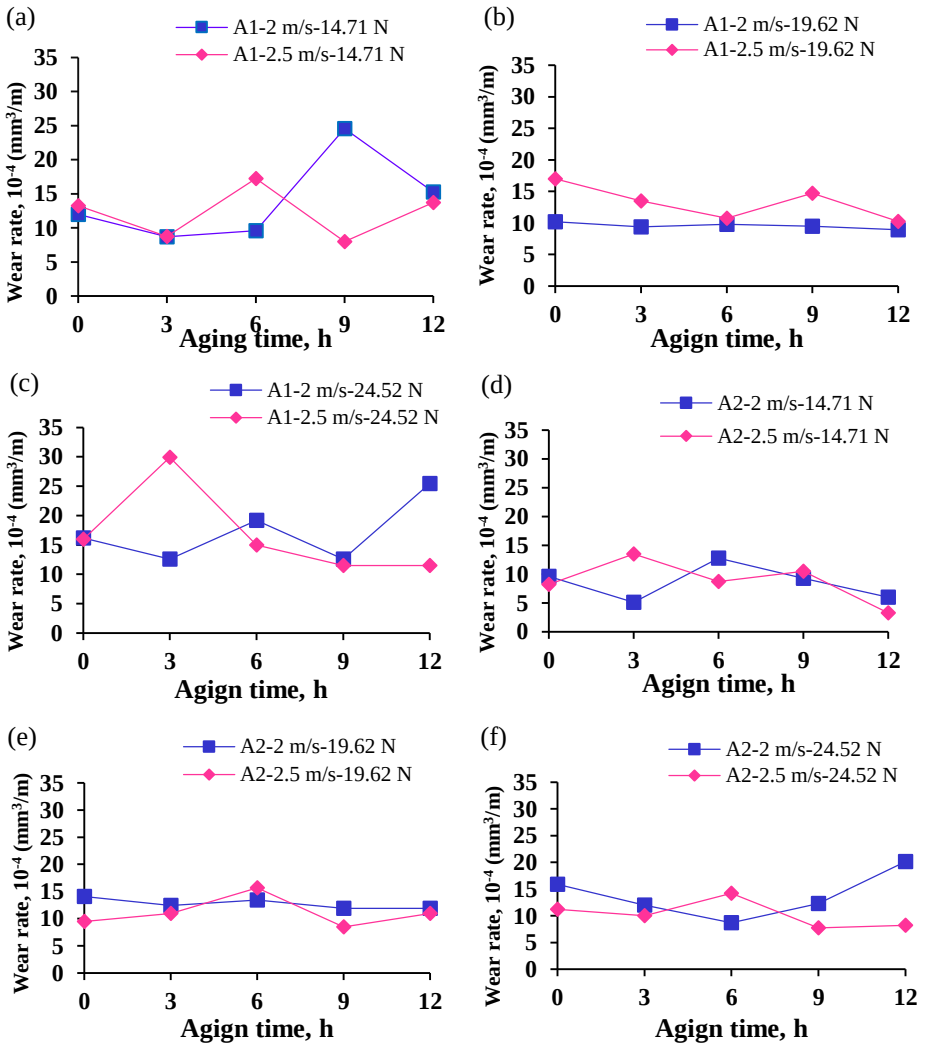

Fig. 7. (a), (b), (c), (d), (e), and (f) are the wear rate of base alloy (Al-Si-Mg – A1) and Composites (Al-Si-Mg/TiB_2 – A2) as a function of ageing time by varying sliding speed (2, 2.5 m/s) and normal applied load (14.71, 19.62, 24.52 N).

At 9 h ageing time, 2 m/s sliding speed, 14.71N load and 3 h ageing time, 2.5 m/s sliding speed, 24.52N load, and the wear rate of the base alloy increases significantly in Figures

7 (a) and (c), respectively. BHN of wear samples is performed to comprehend the phenomenon of uneven wear increment. According to reports, the hardness (average value of five indentations at a different location) of respective samples decreases from 96 to 56 (9 h ageing time) and 89 to 47 (3 h ageing time) BHN after 9 h and 3 h of aging, respectively. Consequently, a significant hardness reduction or work softening phenomenon is responsible for this condition's increased wear rate.

3.3.2 Effect of composition on wear behaviour

Figure 8 compares the wear rates of the Al-Si-Mg system and the Al-Si-Mg/TiB_2 AMC at sliding speeds of 2, 2.5 m/s and applied loads of 14.71, 19.62, and 24.52 N. Fig. 8 (a), (b), and (c) depict the wear behavior of base alloy and composites at 2 m/s as a function of ageing time under a normal applied load of 14.71, 19.62, and 24.52 N. At 14.71 and 24.52 N load conditions, the wear rate of composites decreases with increasing ageing time (greater than 9 hours) when sliding at 2 m/s. Nonetheless, in Fig. 7 (b) at a normal load condition of 19.62 N, the wear rate of the base alloy is less than that of composites. Figure 8 (d), (e), and (f) indicate that as the sliding speed increased by 2.5 m/s, the wear rate of composites with a longer ageing time (greater than 9 h) decreased steadily compared to the base alloy.

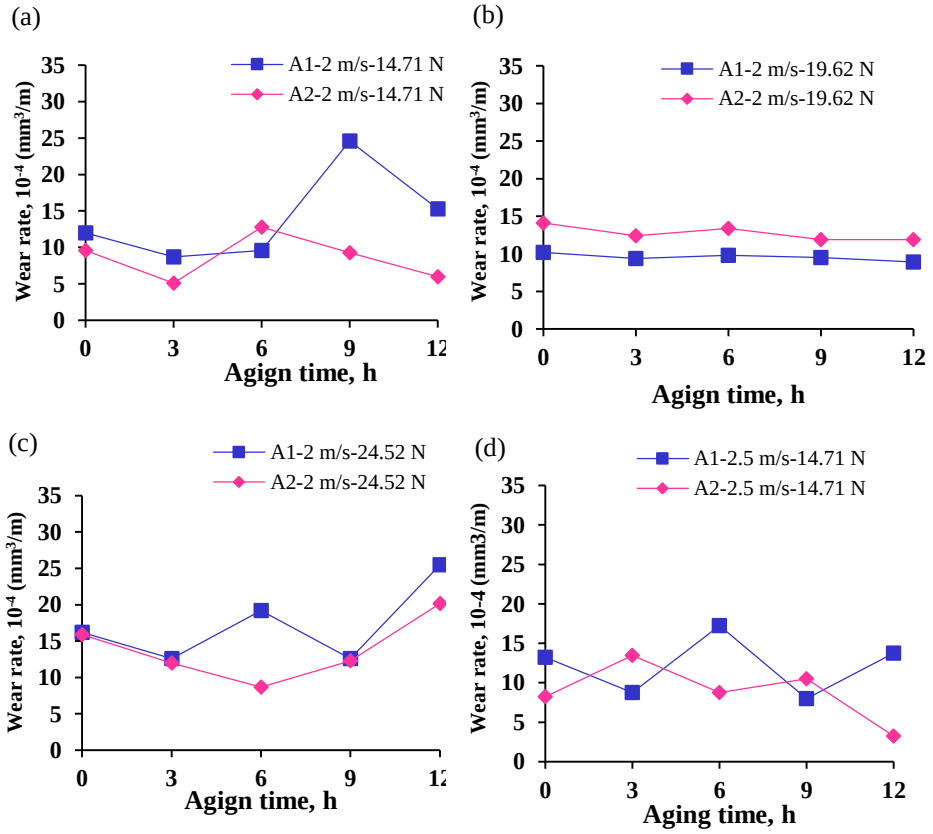

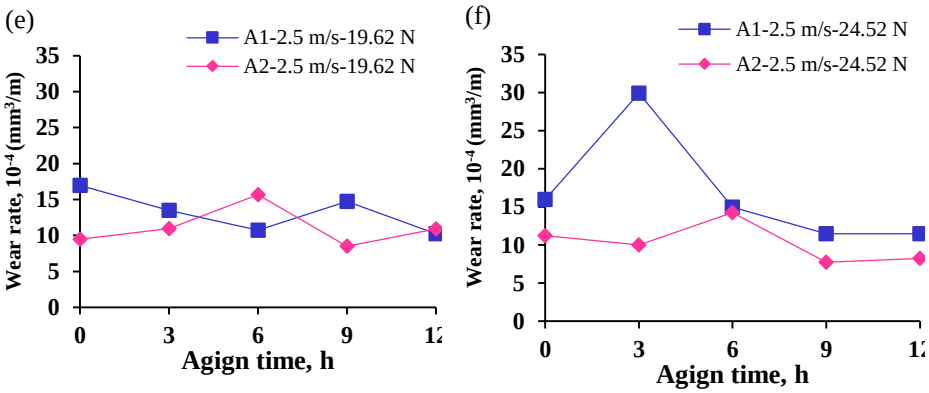

Fig. 8. (a), (b), (c), (d), (e), and (f) are a comparison of base alloy (Al-Si-Mg – A1) and Composites (Al-Si-Mg/TiB_2 – A2) wear rate as a function of aging time by varying sliding speed (2, 2.5 m/s) and normal applied load (14.71, 19.62, 24.52 N).

At the higher aging time (greater than 9 hours) reported in this discussion, wear rate is a function of sliding speed. In most cases, as the sliding speed increased by 2.5 m/s, the wear rate decreased significantly with increased ageing time, with the exception of the 19.62 N normal load condition in the base alloy.

3.4 XPS studies

X-ray photoelectron spectroscopy (XPS) explains the surface's stoichiometry and chemical composition due to its exceptional high surface sensitivity, quantitative nature, and element selectivity [20]. A lower wear rate in composites with a longer ageing time and higher sliding velocity than the base alloy [21]. In order to comprehend the worn surface morphology of Al-Si-Mg/TiB_2 AMC, two representative samples were chosen at different sliding speeds (2 and 2.5 m/s) and a longer ageing time (9 and 12 h). As the valance state of an element increases, the respective element's binding energy also increases. The binding energy of Fe $2p_{3/2}$ was about 709 EV for Fe^{+2} and 711 EV for Fe^{+3}. Fig. 9 (d) shows the XPS peaks of the Fe 2p regions and Fe $2p_{3/2}$ at 709 EV and Fe $2p_{1/2}$ at 720 EV, indicating that Fe^{+2} and Fe^{+3} should be guaranteed, resulting in the development of Fe_3O_4. The satellite peak at about 717 EV was a distinctive peak of saturated Fe^{+3} in γ-Fe_2O_3 (maghemite) [21, 22]. It proposes that Fe_3O_4 nanoparticles were partially oxides, and the increased intensity indicates that Fe^{+2} and Fe^{+3} predominate in the system. When Fe content is transferred from the disc (counterpart) surface to the composite pin, shared Fe atoms and the Fe-containing disc will react to form a mechanically mixed layer on the composite pin surface, thereby reducing the system's wear rate [23].

The Mg 2p peak was located at 54 EV and the Al 2p peak was located at 75 EV. Fig. 9 (a) and (c) demonstrate that as the number of oxidizing layers increases, the number of oxide peaks on the high binding energy side of the primary Mg and Al photoelectron peaks increases significantly.

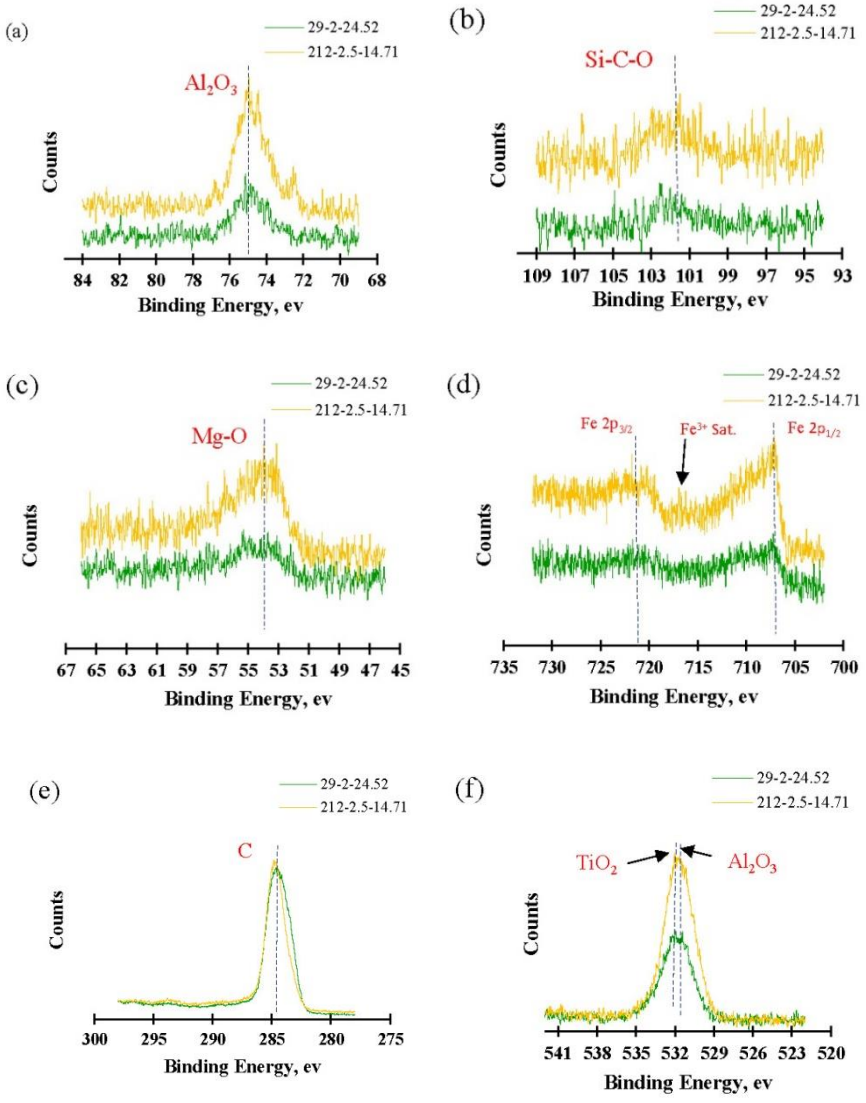

Fig. 9. XPS plots of composites at 9 h artificially aged, sliding speed 2 m/s, load 24.52 N (29-2-24.52) and 12 h artificially aged, sliding speed 2.5 m/s , 14.71 N load (212-2-14.71) (a) Al 2p, (b) Si 2p, (c) Mg 2p, (d) Fe 2p, (e) C 1s, (f) O 1s.

The XPS results detected the peaks allotted to SiO_2, TiO_2, and Al_2O_3. The existence of Si-O implies that Al-Mg-Si has been decomposed and formed oxides during the abrasion process [10]. The XPS results that tribo film formation on the worm surface of Al/TiB_2 mainly due to Al-Mg-Si oxides which reduces the contact of two counterparts

and serves low shear strength junction at the interface [24]. That significantly reduces ploughing between two counterparts, thus reducing the wear rate of the system. That must be responsible for the lower wear rate at higher speed (2.5 m/s), higher load (24.52 N), and ageing time at 9 and 12 h, respectively. Thus the variation in surface composition of worn samples resulted in a change in the wear pattern of pieces. The wear samples' behaviour was incorporated by FESEM-EDS mapping.

3.5 FESEM analysis of worn surfaces

Fig. 10, 11, 12, 13 shows the worn surfaces of AMCs and base alloy at the different ageing times, sliding speed, and applied load. Al-Si-Mg alloy's dry sliding wear rate was reasonably higher than Al-Si-Mg/TiB_2 AMC at ambient temperature in most of the conditions. The overall decrease in AMC's wear rate at lower sliding speed (2.5 m/s) was 37%, and the higher sliding speed (2 m/s) was 4% than the base alloy reported from the results.

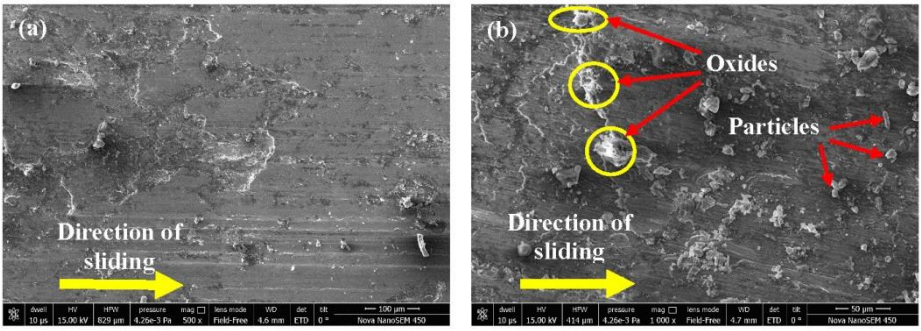

Fig. 10. FESEM images of worn surfaces of the base alloy at 3 h aging time, 2.5 m/s sliding speed and 24.52 N applied load. (a) at lower magnification (b) at higher magnification.

Characteristics of worn surface morphology of AMCs are more complex than those of metals or alloys due to the influence of two major factors: extrinsic factors (normally applied load, sliding speed/distance, temperature, surface finish and hardness of counterpart, nominal contact area) and intrinsic factors (reinforcement size and shape, types, volume/weight fraction, interfacial bonding, porosity, wettability). Therefore, a comprehensive understanding of the wear mechanism is relatively difficult. FESEM-EDS analysis of worn surfaces facilitates the comprehension of AMCs' wear mechanism. Base alloy at 3 h ageing time, 2.5 m/s sliding speed, normal applied load 24.52 N (29.739 x 10^{-4} mm^3/m), AMCs at 9 h ageing, 2 and 2.5 m/s sliding speed, applied load 24.52 N (9.987 x 10^{-4}, 14. 231 x 10^{-4} mm^3/m respectively) and 12 h ageing, 2.5 m/s, applied load 14.71 N (3.245 x 10^{-4} mm^3/m) selected to understand sever, and mild wear mechanism.

3.5.1 Effect of normal applied load

Low and high magnification FESEM micrograph of Al-Si-Mg system at 3 h ageing time, 2.5 m/s sliding speed, and 24.52 N applied load is shown in Fig. 10 (a.) (b). Figure 10 (a) depicts parallel soft ridges and grooves running in the sliding direction; under conditions of high sliding speed and high applied load, there were few delamination

zones. The wear rate of particulate MMCs under varying conditions of normal applied load revealed three wear regimes. In Regime I, under low load conditions, reinforcement particles support the load for which MMCs have a lower wear rate than aluminum alloys. In Regime II, the aluminum alloy and MMC wear rates are identical. Regime III is characterized by the transformation of mild wear to severe wear under high load conditions as the surface temperature exceeds a critical value [3]. As the load applied increased, the wear resistance decreased, and the wear mechanism revealed oxidative layer formation under low load conditions and delamination and adhesion under high load conditions [25]. This conditioning system enables the formation of more stable oxidative layers on the surfaces because the pin on the disc was subjected to wear testing at ambient air temperature [26].

Due to the formation of a sound oxide film on the pin, the amount of abrasion that forms on its surfaces is restricted. Similarly, Fig. 10 (a) depicts deeper observed grooves and ridges in the context of a reported high wear rate. Due to low sliding speed and in-situ TiB_2 particles, AMCs exhibited gross plastic deformation. At a low sliding speed, flakier-shaped particles are ploughed and delamination zones appear, resulting in a higher wear rate.

3.5.2 Effect of sliding speed

Al-Si-Mg and Al-Si-Mg/TiB_2 AMC appear to have relatively high deformation and exposed cracks in the given zone under higher magnification and slower sliding speed (Figs. 10, 11). However, at high sliding speeds and long aging times, AMCs appear to have more minor cracks than base alloy (Fig. 11, 12). AMCs have a low wear rate at higher sliding speeds. It is a result of the formation of a dense oxidative transfer layer on the pin surfaces. In addition, Al-Si-Mg and Al-Si-Mg/TiB_2 composites with a slower siding speed show extreme wear [27]. At a slower sliding speed, Fig. 10 (d) depicts a reduced oxide and Fe transfer. Consequently, at lower sliding speeds, oxidative layers were not stable due to insufficient Fe content transfer from the counterpart to the pin; this circumstance does not permit the formation of sound inter-reactive components. This is responsible for a significant amount of delamination, loose oxide layers, and increased stresses in the disc and pin's contact region.

3.5.3 Effect of ageing time

However, Al-Si-Mg/TiB_2 AMC exhibits a smooth surface morphology at a longer ageing time and higher sliding velocity (Fig. 12, 13). On the surface of specimens, plowing and material flow cause the formation of small globular-shaped particles, small pits, and soft ridges. These phenomena indicate that abrasive wear has occurred under conditions of high sliding speed and long ageing [28]. Transformation of mild wear to severe wear depends on sliding speed and ageing time, but also on the combined effect of other parameters such as particle size and shape, volume/weight fraction of reinforcements, temperature, and formation of new phases at interfaces.

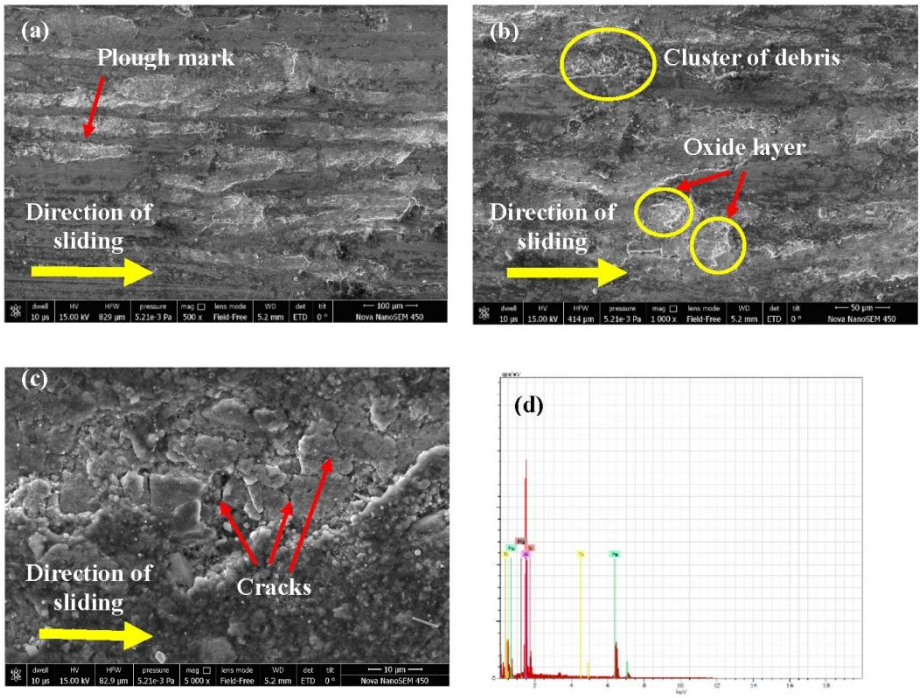

Fig. 11. (a), (b), (c) FESEM images of Al-Si-Mg/TiB_2 composites at 9 h ageing time, 2 m/s sliding speed and 24.52 N, (d) EDS mapping of Al-Si-Mg/TiB_2 composites at 9 h ageing time, 2 m/s sliding speed and 24.52 N.

3.5.4 Effect of hardness

The response of the base alloy and the hardness of AMC is depicted in Figure 6. The test samples' hardness is a function of their aging time. In comparison to AMC, the hardness of the base alloy increases as ageing time increases. However, increasing hardness diminishes the rate of wear. In addition, experimental evidence suggests that the adhesive process slowed the scuffing and seizing of mating counterparts with greater hardness [10]. Fig. 6 depicts the effect of composition on wear behaviour; under lower sliding speed conditions, base alloys exhibit a lower wear rate than composites up to 6 h of ageing time. Moreover, as ageing time and sliding speed increase, the base alloy's wear rate increases in contrast to composites. In addition, XPS results confirm that at higher sliding speeds (2.5 m/s) and longer aging times (12 h), the amount of MML (mechanically mixed layer) significantly increases between counterparts and reduces wear intensity.

3.6.4 Effect of MML (mechanically mixed layer)

Mandal A. et al. (2009) investigated the wear mechanism and achieved wear of Al-Si-Mg/TiB2 in situ composites through the following steps [26];

$$\text{Delamination} \longrightarrow \text{Disintegration} \longrightarrow \text{Simultaneous interaction} \longrightarrow$$
$$\longrightarrow \text{Formation of complex (Al} - \text{Si} - \text{Fe} - \text{Ti) phase (MML)}$$

Woydt M. (2000), *Huang Z. et al.* (2007), and *Xu Z. et al.* (2014) reported that disintegration and simultaneous interaction result in the formation of a complex oxidative Al-Si-Fe-Ti phase (MML). At low and high loads, mild and severe wear mechanisms were reported, respectively. The development of MML at higher sliding speeds and longer aging times restrains material loss by depressing the contact surfaces of the disc and the pin, which is susceptible to mild wear.

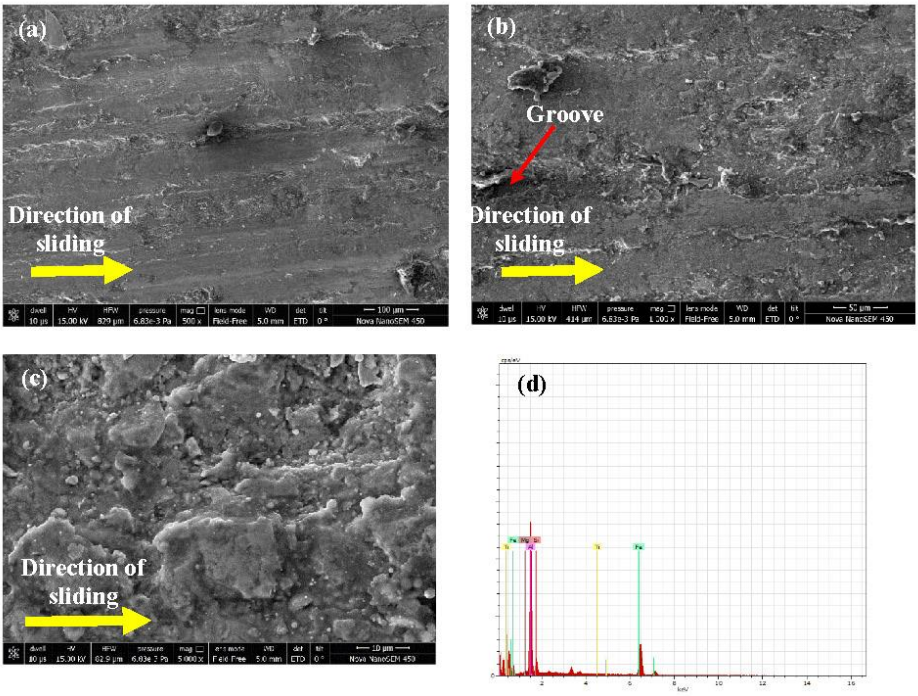

Fig. 12. (a), (b), (c) FESEM images of Al-Si-Mg/TiB_2 composites at 9 h ageing time, 2.5 m/s sliding speed and 24.52 N, (d) EDS mapping of Al-Si-Mg/TiB_2 composites at 9 h ageing time, 2.5 m/s sliding speed and 24.52 N.

Al-Mg-Si oxides reduce contact between two counterparts and serve as a low shear strength junction at the interface, according to an XPS analysis of two composites subjected to a higher load and a higher sliding speed over a period of 12 hours. This significantly reduces the amount of plowing between the two halves, thereby decreasing the system's wear rate.

Fig. 9 reported that as ageing time increased peak of oxides or MML on the surfaces significantly increased. It was a reasonably reduced wear rate.

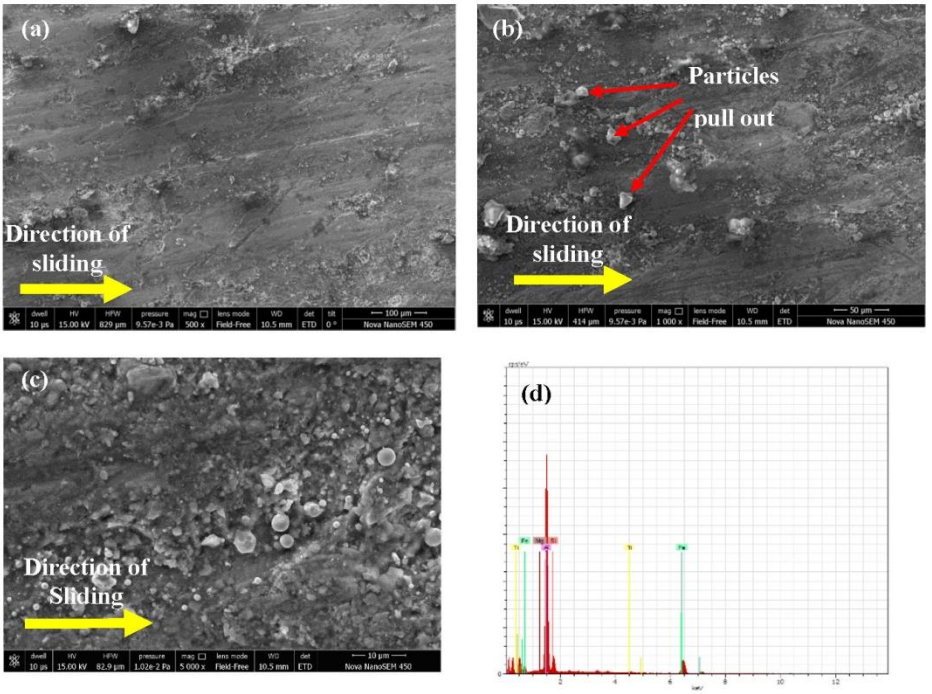

Fig. 13. (a), (b), (c) FESEM images of Al-Si-Mg/TiB_2 composites at 12 h ageing time, 2.5 m/s sliding speed and 14.71 N, (d) EDS mapping of Al-Si-Mg/TiB_2 composites at 12 h ageing time, 2.5 m/s sliding speed and 14.71 N.

During dry sliding, the hard ceramic (TiB_2) particles easily abraded graphite flakes and Fe particles from the disc surface, resulting in the oxidation of the pin surface and the formation of an even thin layer of Al_2O_3, TiO_2 [22, 23], SiO_2, Fe_2O_3, Fe_3O_4 [21, 22] base compound on the pin surface. The transfer rate of graphite flakes and Fe increased with the dispersion AMCs of TiB_2 particles; extended aging time and high sliding velocity-based AMCs were observed in this type of phenomenon [29, 30].

Particle formation and reinforcement dispersion in the system substantially improved the dimensional stability of AMCs. Peak aging conditions altered the morphology of α-Al and Si. As α-Al dendrites become smaller or modified, the peak strain and hardening rate for similar alloys increase dramatically [31]. Consequently, ageing and TiB_2 enhance work hardening and wear resistance at higher loads and speeds. In addition, the formation of iron-rich oxides or MML reduced the rate of wear in AMCs [32].

In addition, the coefficient of thermal expansion of TiB_2 (7×10^{-6} K^{-1}) is three-time lesser than aluminium (24×10^{-6} K^{-1}), it is leading to a considerable amount of strain at the matrix-particle interfaces, and that is relieved by the development of dislocations [15]. This is one reason to increase the dislocation density in the AMCs, which significantly boosts the strength and aging kinetics. Simultaneously increasing load and sliding speed increases the formation of MML in the system. As a portion of the particle formation

increases, the uniform distribution of reinforcements and formation of MML improves wear resistance by reducing the disc and pin's contact surfaces [33].

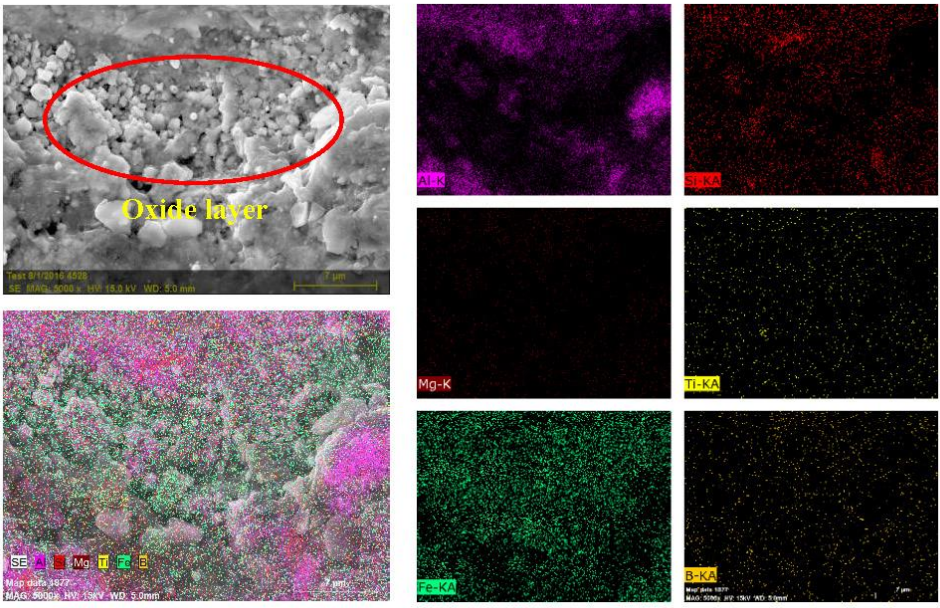

Fig. 14. EDS mapping of Al-Si-Mg/TiB_2 composites at 9 h ageing time, 2.5 m/s sliding speed and 24.52 N.

According to the results, the transfer layer (MML) acted as a protective layer on the pin surface and reduced the wear rate. Transitions in sliding distance, load, and sliding speed induce mild and severe wear. TiB_2 serves as a wear-resistant load-carrying material at higher loads and sliding speeds because MML is compromised [34, 35]. The wear rate decreases as the ageing time, sliding speed, and applied load conditions increase. Literature reports that the base alloy attained primary hardening phases after 3 to 4 hours of aging. After 6-12 hours of aging, a few more precipitate phases developed in AMCs, which dominated the significant increase in hardness and were responsible for the lower wear rate in composites with longer aging times [34]. The EDS analysis revealed a dense layer of MML on the worn surfaces of composites with longer aging times and faster sliding speeds.

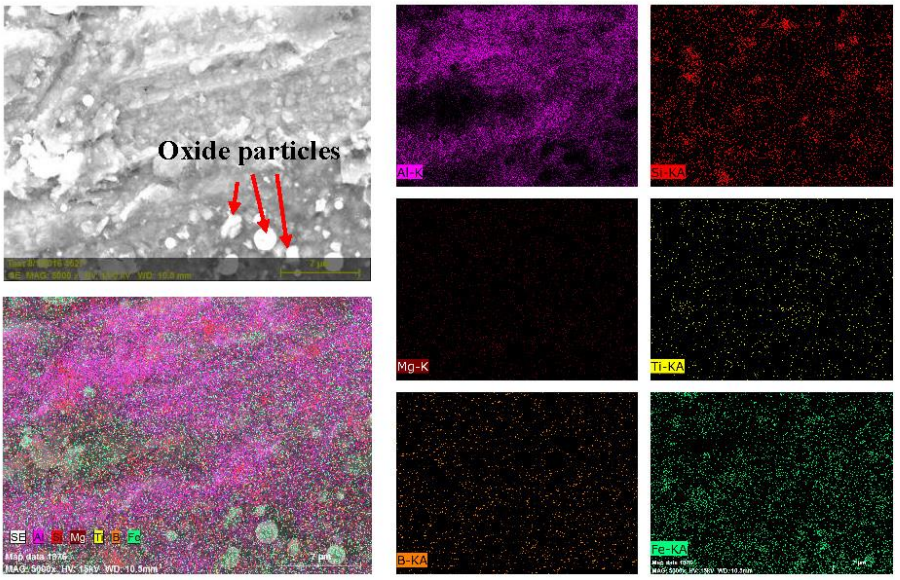

Fig. 15. EDS mapping of Al-Si-Mg/TiB_2 composites at 12 h ageing time, 2.5 m/s sliding speed and 14.71 N.

Variable process parameters can be used to attribute fluctuations in the wear rate of composites compared to the base alloy to a complex reaction system during dry sliding conditions. This leads to a comprehensive examination and study of the microstructure formed during the wear process. However, the following explains the Al-Si-Mg/TiB_2 AMCs' wear mechanism.

Table 1. Mode of wear and wear mechanism.

Mode of wear	Mild wear	Severe wear
FESEM images of worn surfaces		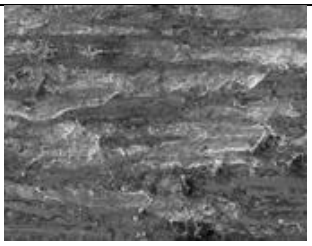
Wear mechanism and condition	• Abrasive wear and MML have drawn plough and groove, mild delamination with MML on worn surfaces. • As discussed above, mild wear appears due to low applied load, high sliding speed, and high ageing time.	• The metal flow was responsible for gross plastic deformation, and as a result, it removed MML layers from the worn surfaces. • Severe wear appears due to high applied load, low sliding speed, and low ageing time, as discussed above.

Conclusion

An artificially aged Al-Si-Mg alloy and Al-Si-Mg/TiB_2 AMCs selected for the wear studies by varying sliding speed (2, 2.5 m/s) and normal applied load (14.71, 19.62, 24.52 N). The investigation draws the following conclusions.

a.) XRD results reported forming in situ TiB_2 particles in the alloy system and forming Al_3Ti and AlB_4 intermetallics. Micrographs results show uniform particle distribution of TiB_2 in the system.

b.) The overall decrease in AMCs wear rate at higher sliding speed (2.5 m/s) was 37%, and lower sliding speed (2 m/s) was 4% than the base alloy reported from the results. Work hardening due to in situ ceramic (TiB_2) reinforcement and ageing substantially decreases wear rate. However, in base alloy at some point work softening is reported (Fig. 7 (a), and (c)).

c.) The FESEM fractography of worn surfaces of AMCs reported mild ridges, grooves and ploughed at mild wear (2.5 m/s, 14.71 N) and severe wear (2 m/s and 24.52 N) observed gross plastic deformation due to high metal flow.

d.) Combined FESEM-EDS and XPS analysis reveal that the formation of MML or oxidative layers on the worn surfaces reduces the wear rate at the higher ageing time, high sliding speed, and low applied load condition.

e.) However, hardness of base alloy is higher than composites but reasonable wear rate is decreased due to ceramic reinforcements (TiB_2), aging and significant amount of MML and oxidative layers formation and it is increased with sliding speed increased.

f.) The wear rate of composites is a function of ageing time, sliding speed, and applied load.

At the higher ageing time (12 h), high sliding speed (2.5 m/s) and low applied load (14.71 N) attributed to the lowest wear rate.

Acknowledgements

The author appreciatively acknowledges the support of MRC, MNIT, Jaipur, ACMC Department of IIT-Kanpur, and CIF Department, IIT Gandhinagar for metallurgical characterization and TEQIP sponsored High-Pressure High-Temperature Press program at S V National Institute of Technology.

References:

[1] J. Xu, W. Liu: Wear, 260(4-5) (2006) 486-492.
[2] N. R. Rathod, J. Menghani: Metall Mat Eng, 25 (3) (2019) 195-208.
[3] P. Samal, P. R. Vundavilli, A. Meher, & M. M. Mahapatra: J Manu Pro 59 (2021) 131-152.
[4] R. K. Arya, & A. Telang: Int J Eng Adv Technol, 9 (2020) 3366-3374.
[5] A. D. Sarkar, J. Clarke: Wear, 75(1) (1982) 71-85.
[6] S. L. Pramod, S. R. Bakshi, B. S. Murty: J Mat Eng Perform, 24 (6) (2015) 2185-2207.
[7] F. Chen, F. Mao, Z. Chen, J. Han, G. Yan, T. Wang, Z. Cao: J Alloy Compd, 622 (2015) 831-836.
[8] B. M. Viswanatha, M. P. Kumar, S. Basavarajappa, T. S. Kiran: Tribol Ind, 36 (1) (2014) 40-48.

[9] C. A. Caracostas, W. A. Chiou, M. E. Fine, H. S. Cheng: Metall Mat Trans A, 28 (2) (1997) 491-502.
[10] C. S. Ramesh, A. Ahamed: Wear, 271(9-10) (2011) 1928-1939.
[11] S. M. Ma, P. Zhang, G. Ji, Z. Chen, G. A. Sun, S. Y. Zhong, V. Ji, H. W. Wang: J Alloys Compd, 616 (2014) 128-136.
[12] H. Möller, G. Govender, W. E. Stumpf: Int J Cast Met Res, 20(6) (2007) 340-346.
[13] G. A. Edwards, K. Stiller, G. L. Dunlop: M. J. Couper: Act Mat, 46 (11) (1998) 3893-3904.
[14] M. Werinos, H. Antrekowitsch, T. Ebner, R. Prillhofer, P. J. Uggowitzer, S. Pogatscher: Mat Des 107 (2016) 257-268.
[15] K. Pavitra, R. Mitra: Mat Sci Eng A, (2012) 557 84-91.
[16] S. Lakshmi, L. Lu, M. Gupta: J Mat Process Tech, 73(1-3) (1998) 160-166.
[17] S. K. Shaha, F. Czerwinski, W. Kasprzak, J. Friedman, & D. L. Chen: Mat Sci Eng A, 652 (2016) 353-364.
[18] N. L. Yue, L. Lu, M. O. Lai: Struct, 47(1-4) (1999) 691-694.
[19] K. Niranjan, P. R. Lakshminarayanan: Mat Des, 47 (2013) 167-173.
[20] I. Bertoti: Surf Coat Tech, 151 (2002) 194-203.
[21] S. Gota, E. Guiot, M. Henriot, M. Gautier-Soyer: Phy Rev B, 60(20) (1999) 14387.
[22] P. Li, E. Y. Jiang, H. L. Bai: J Phy D: App Phy, 44 (7) (2011) 075003.
[23] P. L. Menezes, S. V. Kailas: Wear, 265 (11-12) (2008) 1655-1669.
[24] Z. Xu, X. Shi, Q. Zhang, W. Zhai, J. Yao, L. Chen, Q. Zhu, Y. Xiao: J Mat Eng Perform, 23(6) (2014) 2255-2264.
[25] F. Gul, M. Acilar: Comp Sci Tech, 64(13-14) (2004) 1959-1970.
[26] A. Mandal, B. S. Murty, M. Chakraborty: Wear, 266(7-8) (2009) 865-872.
[27] K. M. Shorowordi, A. S. M. A. Haseeb, J. P. Celis: Wear, 256 (11-12) (2004) 1176-1181.
[28] I. Kakaravada, A. Mahamani, V. Pandurangadu: Int J Mat Eng Innov, 11(2) (2020) 145-162.
[29] J. Singh, A. T. Alpas: Metall Mat Trans, A 27(10) (1996) 3135-3148.
[30] B. Venkataraman, G. Sundararajan: Wear, 245(1-2) (2000) 22-38.
[31] Q. G. Wang, C. H. Caceres: Mat Sci Eng: A, 234 (1997) 106-109.
[32] A. S. Vivekananda, S. B. Prabu: Tribo Lett, 66 (1) (2018) 1-14.
[33] S. Suresh, N. S. V. Moorthi, S. C. Vettivel, N. Selvakumar: Mat Des, 59 (2014) 383-396.
[34] Y. Shen, T. Hong, J. Geng, G. Han, D. Chen, X. Li, H. Wang: Mat Chart, 124 (2017) 25-30.
[35] S. D. Kumar, A. Mandal, M. Chakraborty: Mat Sci Eng: A, 636 (2015) 254-262.